CRYSTALLOGRAPHY REPORTS, 2025, Vol. 70, No. 1, pp. 60–65

PHYSICAL PROPERTIES OF CRYSTALS

ATOMISTIC SIMULATION OF PARATELLURITE α–TeO_2 CRYSTAL. II. ANISOTROPY AND MICROSCOPIC ASPECTS OF ION TRANSPORT

© 2025 A. K. Ivanov-Schitz*

Shubnikov Institute of Crystallography, Kurchatov Complex of Crystallography and Photonics, National Research Centre "Kurchatov Institute", Moscow, Russia

**e-mail: alexey.k.ivanov@gmail.com*

Received July 16, 2024
Revised July 31, 2024
Accepted July 31, 2024

Abstract: The molecular dynamics simulation was used to study the peculiarities of ion transport in α–TeO_2 paratellurite crystals. It has been shown that in α-TeO_2, ion transport caused by oxygen transport is anisotropic. The highest values of diffusion coefficients are observed along the *c*-axis and amount to: $D_O \sim 1\times10^{-7}$ cm^2/s at temperatures near the melting point. It has been shown that oxygen ions jump over distances of 1.5–2.5 Å via a vacancy or interstitial mechanism.

DOI: 10.31857/S00234761250108e7

INTRODUCTION

Paratellurite (tetragonal α-phase TeO_2) [1–3] has a wide range of physical characteristics and is used in various optical devices [4, 5], ultra-high integration electronic devices [6], gas sensors [7], and as an X-ray optical adaptive element [8, 9]. The operation of the X-ray optical adaptive element is based on the effect of changing diffraction peaks when an electric field is applied to the crystal, which is apparently associated with the migration of ion carriers in the near-surface layers of paratellurite, but a detailed analysis of ion transport processes has not been carried out to date.

In this work, using computer simulation by the molecular dynamics (MD) method, the features of ion transport in defect α-TeO_2 crystals containing either oxygen and tellurium ion vacancies or interstitial oxygen ions are considered. The main attention was paid to the microscopic analysis of ion migration and the study of the anisotropy of ion transport in different crystallographic directions.

METHODS AND APPROACHES

For the MD simulation, a computational cell (box) was formed containing 980 Te atoms and 1960 O atoms, but taking into account the presence of nuclei and electron shells, the total number of simulated particles is doubled to 5880 "particles". Point defects (oxygen vacancies and interstitial oxygen ions) were created in the system, as described in detail in [10]. A detailed description of the MD simulation parameters is given in the same work.

DISCUSSION OF RESULTS

Ion transport anisotropy. In this study, only oxygen-ion transport was investigated, since, as was shown earlier [10], the formation of cation defects is energetically unfavorable. In addition, tellurium diffusion was not observed in any of the studied defect systems: this means that $D_{Te} << 10^{-10}$ cm^2/s [10]. The absence of tellurium diffusion is consistent with experimental data on NMR (Te) [11, 12], from which it follows that $D_{Te}(950\ \text{K}) < 10^{-15}$ cm^2/s.

Figure 1 shows the temperature dependences of the oxygen diffusion coefficients measured along the crystal axes of defective crystals of different types – with vacancies and interstitial oxygen atoms. For both types of defects, the highest oxygen mobility is observed in measurements along the *c* axis, with diffusion along the *a*, *b* axes being approximately 1.5 times smaller.

The activation energies of the diffusion (E_D) depend quite strongly on the nature of the defects of the samples: in crystals containing interstitial oxygen ions, the E_D value is approximately half the similar values for crystals with vacancy disorder.

The weakly changing value of the diffusion activation energy along different crystallographic directions is noteworthy: about 0.75 eV for a crystal with vacancies and 0.42 eV for samples with interstitial defects. Figure 2 shows the migration maps obtained using the PathFinder program [13] for oxygen ions

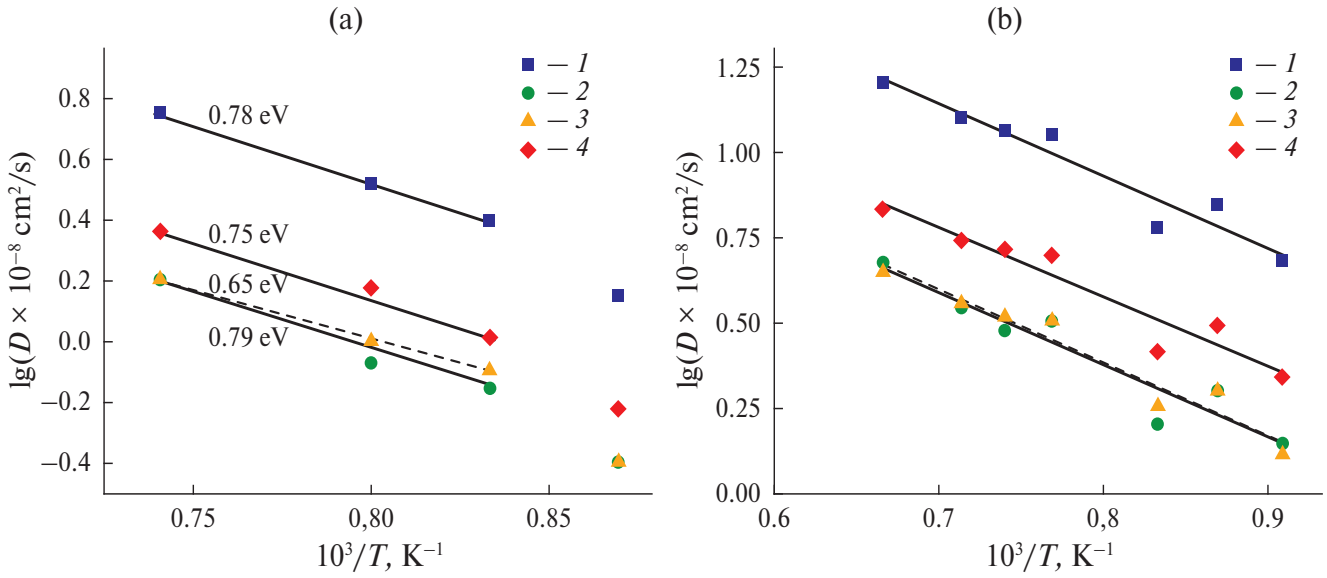

Fig. 1. Temperature dependences of the oxygen diffusion coefficients D_O in crystals containing 15 oxygen vacancies (a) and 10 interstitial oxygen ions (b): total diffusion coefficient (1), D_O along the axes *a* (2), *b* (3) and *c* (4), respectively. The numbers near the straight lines are the diffusion activation energies.

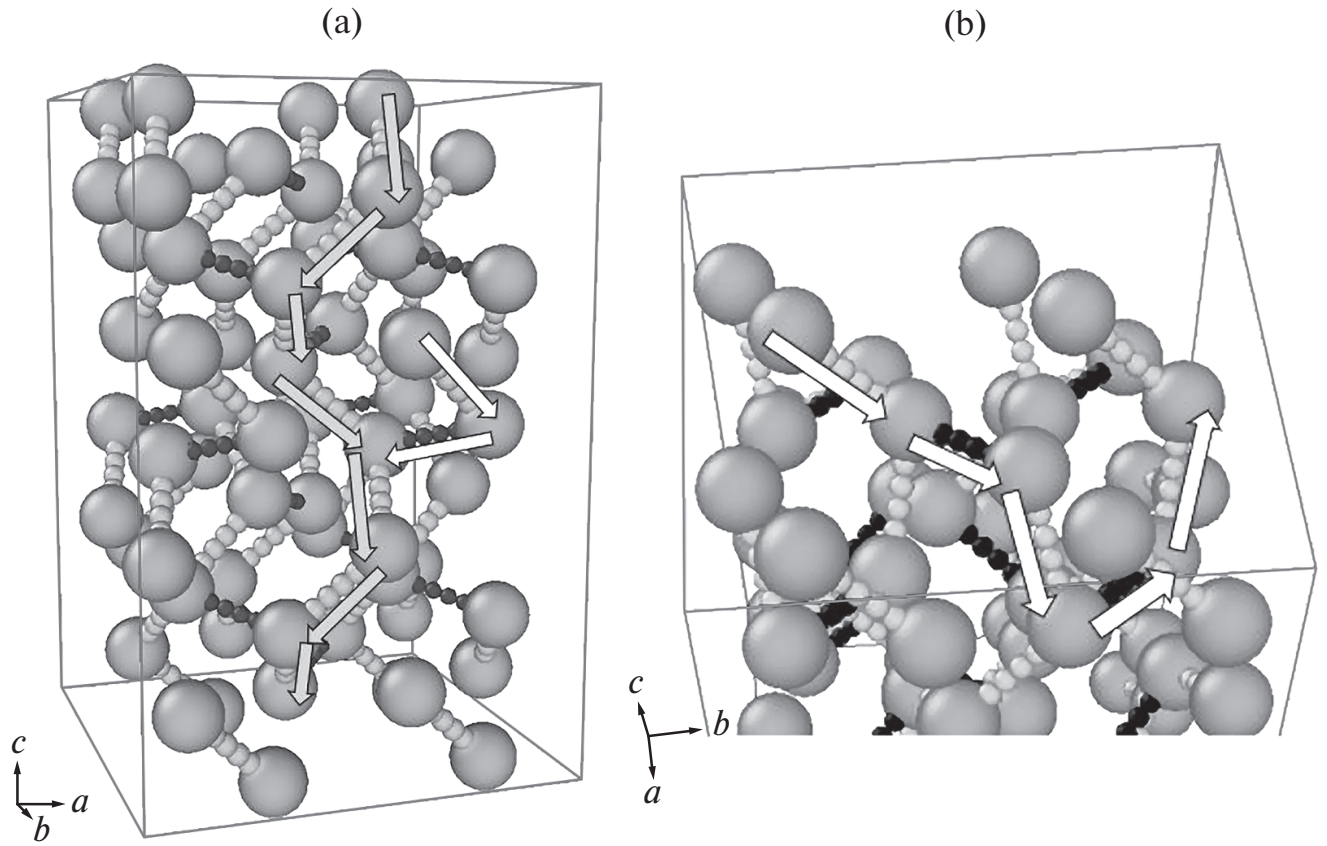

Fig. 2. Possible transport routes of oxygen anions. Large spheres are oxygen in crystallographic positions, small grey and black spheres are possible intermediate positions of oxygen for "channels" of two types. Arrows show possible trajectories of oxygen movement in the direction of the *c* axis (a) and in the directions of the axes *a*, *b* (b).

of a defect-free paratellurite crystal. Note that the pathfinding procedure is based on the analysis of distances between the nearest neighbors and the crystallographic symmetry of the atomic positions. As can be seen from Fig. 2a, the oxygen vacancy transport along the *c* axis can be carried out in two ways, including either "channels" of one type (the possible trajectory of O^{2-} movement is shown by gray arrows) or "channels" of two different types (the possible trajectory of O^{2-} movement is shown by white arrows). "Channels" of two types are involved in the movement of oxygen along the *a*- and *b*-axes (Fig. 2b). Note that in this case the trajectory is complicated and does not belong to the plane (*a*–*b*), but includes mandatory transitions in the direction of the *c* axis. However, for a more detailed analysis of possible transport paths (and especially the values of the diffusion activation energy), additional studies are necessary taking into account the defective structure of the crystals, especially in the case of the introduction of additional interstitial oxygen ions.

As was indicated in [10], in α-TeO_2 crystals, along with ionic conductivity, electron-hole conductivity is observed, which is confirmed by the results of direct measurements of the electrical conductivity (σ) of paratellurite single crystals [15, 16], and in the low-temperature region ($300 < T < 500$ K) the conductivity is due to the migration of "impurity" oxygen vacancies. To verify the above assumptions, estimates of the ionic conductivity values were made within the framework of the simplest hopping model. Considering that the electrical conductivity is due to the excess concentration of either vacancies (n_V) or interstitial ions (n_{int}), we have, respectively:

$$\sigma_V = \frac{n_V D_V q_O^2}{kT} \text{ and } \sigma_{\text{int}} = \frac{n_{\text{int}} D_{\text{int}} q_O^2}{kT}. \quad (1)$$

Here n_V (n_{int}), D_V(D_{int}) are the concentrations and diffusion coefficients of vacancies and interstitial oxygen ions, respectively.

Extrapolating the data shown in Fig. 1 to a temperature of 300 K, we obtain:

$$D_V\,(300\,\text{K}) = 5.3 \cdot 10^{-18}\text{cm}^2\ /\text{s},$$

$$D_{\text{int}}\,(300\,\text{K}) = 3.5 \cdot 10^{-13}\text{cm}^2/\text{s}.$$

The conductivity values calculated according to (1) are:

$$\sigma_V\,(300\,K) \approx 5 \cdot 10^{-14}\,\text{S/cm};$$

$$\sigma_{\text{int}}\,(300\,K) \approx 10^{-8}\,\text{S/cm}.$$

Experimental values of electrical conductivity at room temperature vary within the range of (4–20) × 10^{-14} S/cm [9, 14, 15]. Thus, it can be considered that the hypothesis of the vacancy mechanism of oxygen-ion conductivity receives additional justification.

Microscopic aspects of ion transport. To visualize the features of anion transport, the trajectories of oxygen motion in samples with different defects were analyzed. In all defect crystals, most of the oxygen ions move around their crystallographic positions (Figs. 3a, 4a), and the amplitude of thermal oscillations found from the analysis of histograms of atomic positions (Figs. 3b, 4b) is 0.7–0.8 Å, which is in good agreement with the data obtained from the analysis of root-mean-square displacements: 0.65–0.75 Å.

In defect systems, a number of oxygen anions were found that perform jumps to vacant positions, as shown in Fig. 2c, 2e–3c, 3e. There are two types of "jumps". First, the jump occurs by approximately 1.2–1.5 Å in a few picoseconds with the possibility of returning to the initial position (Fig. 3c–4c). Second, the jump can occur quickly (in 0.5–1 ps) over a distance twice as large, i.e., by 2.2–2.5 Å (Fig. 3f, d–4f, d).

The ions involved in the charge transport are located in the volume of the modeled system, as a rule, randomly. However, sometimes situations can be observed when the "jumping" oxygen anions are close to each other (Fig. 5). But even in this case, no consecutive jumps are observed, i.e. these are not correlated jumps.

Using the simplest diffusion model, we can estimate the value of the diffusion coefficient of D_O (at 1200–1400 K) by taking the average jump length (l = 1.5–2.5 Å) and assuming that during the calculated time (500–800 ps) the oxygen ion made one jump, i.e. the jump frequency was (ν = 1.3–2) × 10^9 Hz:

$$D_O = \left(\frac{1}{6}\right) l^2 \nu = (5 - 20) \cdot 10^{-8}\ \text{cm}^2/\text{s}\ .$$

The calculated diffusion coefficients are in good agreement with the values obtained from the analysis of root-mean-square displacements: D_O = (5–10) × 10^{-8} cm^2/s.

CONCLUSION

MD modeling allowed us to determine that in α-TeO_2 paratellurite crystals, both vacancies and interstitial oxygen anions are involved in ion transport processes. The hopping mechanism is described by two types of "jumps": a jump of approximately 1.2–1.5 Å in a few picoseconds with the possibility of returning to the initial position, or fast (0.5–1 ps) jumps over twice the distance. The highest oxygen mobility is observed in measurements along the *c* axis, with diffusion along the *a*, *b* axes decreasing by approximately 1.5 times.

ACKNOWLEDGMENTS

The author expresses gratitude to Yu.V. Pisarevsky for his interest and attention to the work.

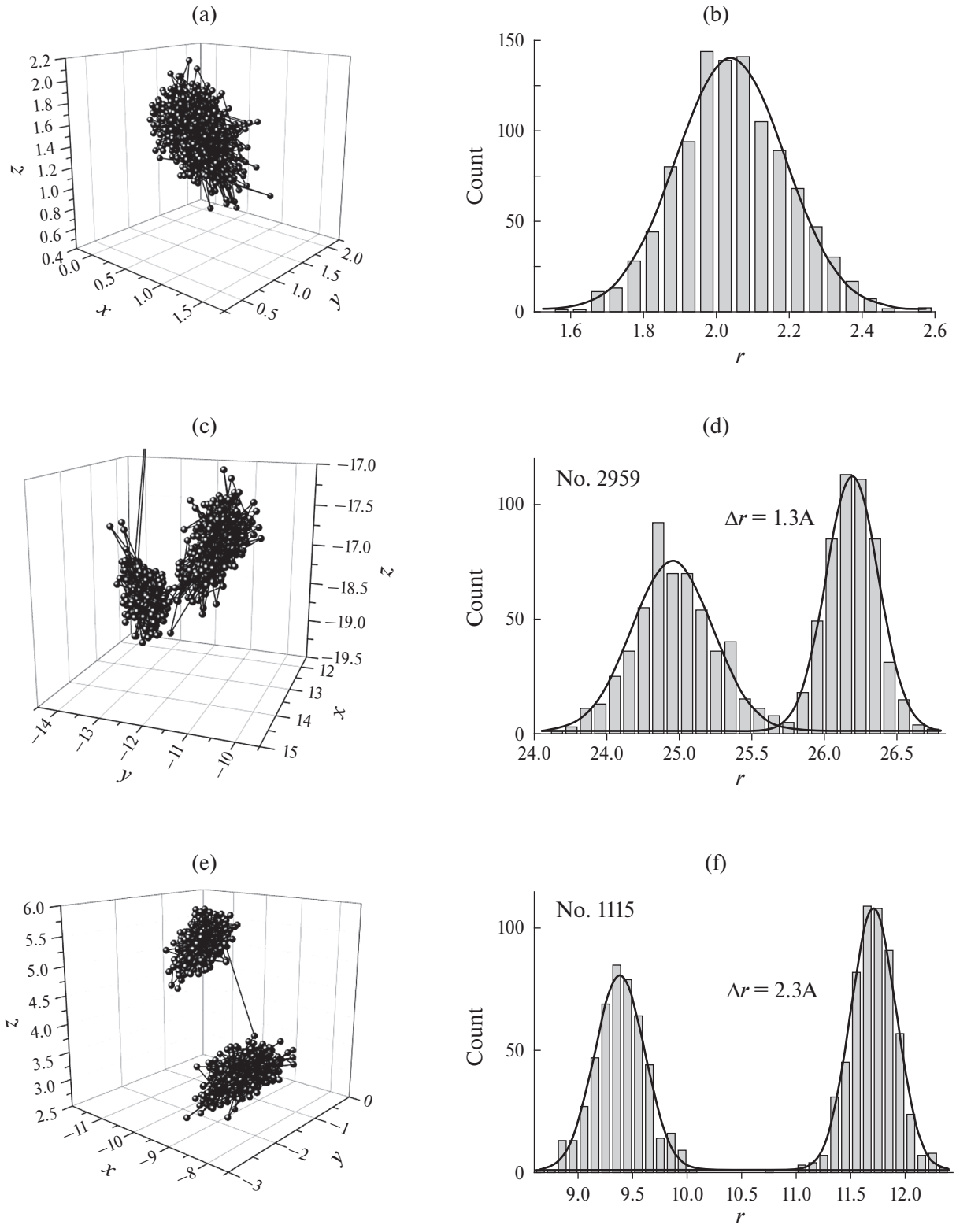

Fig. 3. Calculated trajectories of oxygen anions in a TeO_2 crystal with 15 oxygen vacancies.

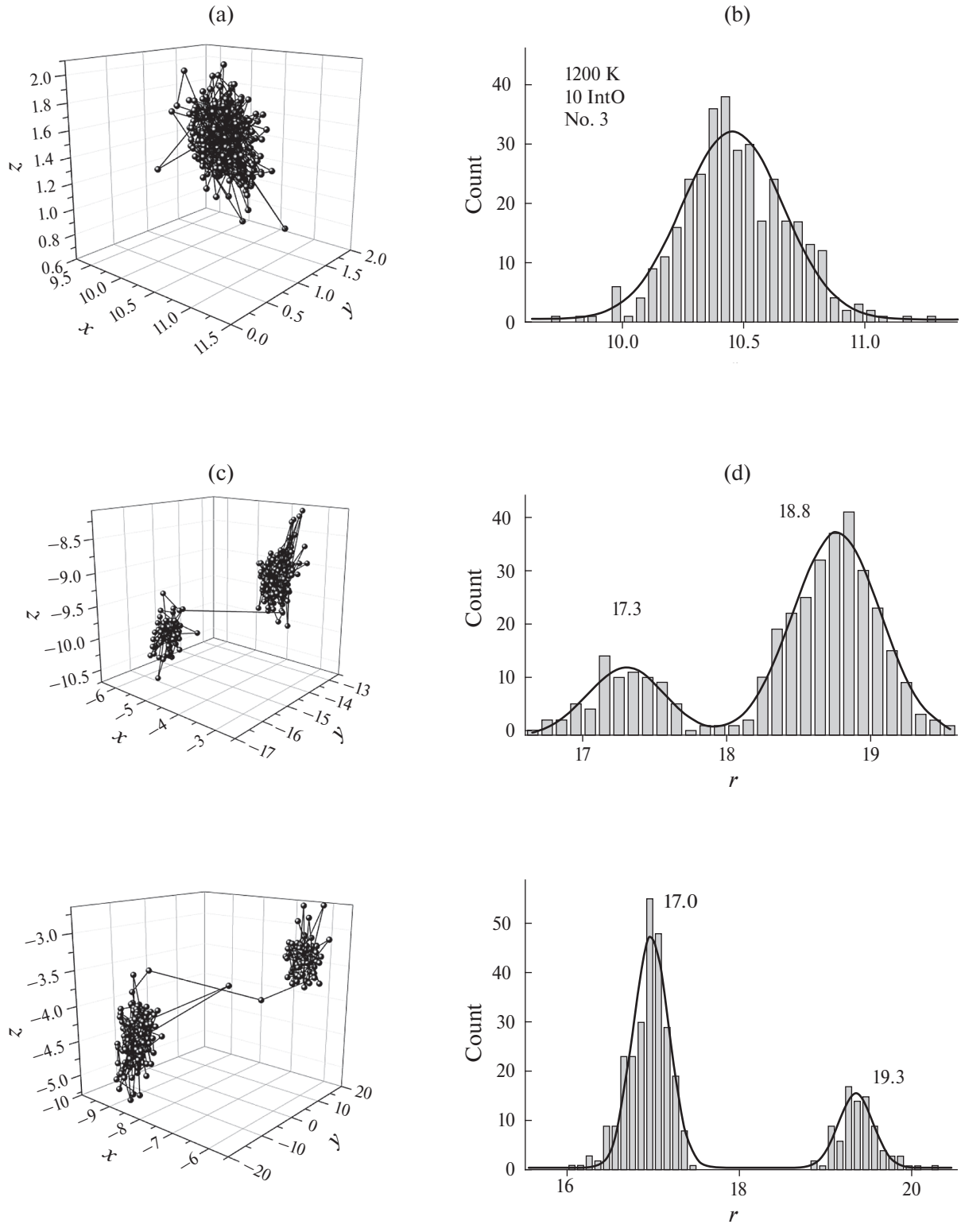

Fig. 4. Calculated trajectories of oxygen anions in a TeO_2 crystal with 10 interstitial oxygen atoms.

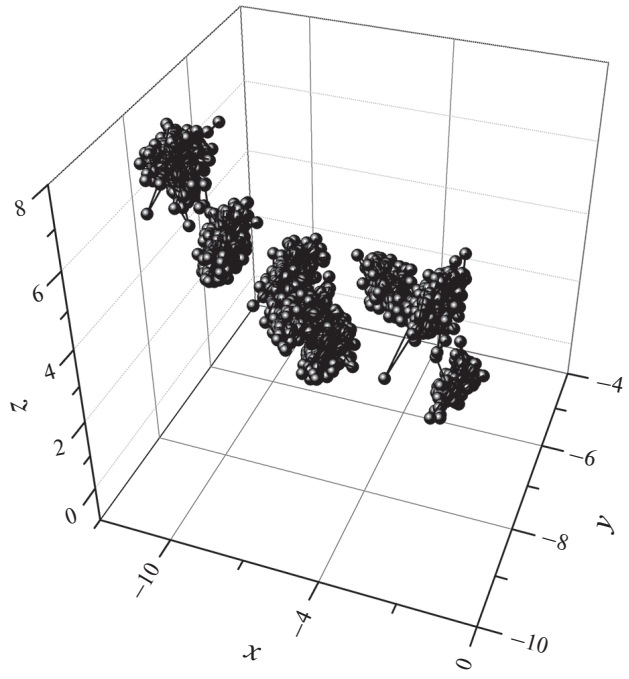

Fig. 5. Three adjacent uncorrelated jumps of oxygen anions.

FUNDING

The work was carried out according to the State assignment of the National Research Center "Kurchatov Institute".

REFERENCES

1. *Kondratyuk I.P., Muradyan L.A., Pisarevsky Yu.V. et al.* // Crystallography. 1987. V. 32. P. 609.
2. *Thomas P.A.* // J. Phys. C. 1988. V. 21. P. 4611. http://stacks.iop.org/0022–3719/21/i=25/a=009
3. *Dudka A.P., Golovina T.G., Konstantinova A.F.* // Crystallography. 2019. V. 64. P. 930. https://doi.org/10.1134/S0023476119060043
4. *Arlt G., Schweppe H.* // Solid State Commun. 1968. V. 6. P. 783. https://doi.org/10.1016/0038–1098(68)90119–1
5. *Wang P., Zhang Z.* // Appl. Opt. 2017. V. 56. P. 1647 https://doi.org/10.1364/AO.56.001647
6. *Li Y., Fan W., Sun H. et al.* // J. Appl. Phys. 2010. V. 107. P. 093506. https://doi.org/10.1063/1.3406135
7. *Liu Z., Yamazaki T., Shen Y. et al.* // Appl. Phys. Lett. 2007. V. 90. P. 173119. https://doi.org/10.1063/1.2732818
8. *Kovalchuk M.V., Blagov A.E., Kulikov A.G. et al.* // Crystallography. 2014. V. 59. P. 950.
9. *Kulikov A.G.* Formation of surface structures in crystals of lithium paratellurite and tetraborate during migration of charge carriers in an external electric field. Diss. ... Cand. of Phys. and Mathematics. Moscow, 2019.
10. *Ivanov-Shits A.K.* //Crystallography. 2024. V. 69. No. 6. P. (in print).
11. *Wegener J., Kanert O., Küchler R et al.* // Z. Naturforsch. A. 1994. V. 49. P. 1151. https://doi.org/10.1515/zna-1994-1208
12. *Wegener J., Kanert O., Küchler R. et al.* // Radiat. Eff. Defects Solids. 1995. V. 114. P. 277.
13. BatteryMaterials. https://pathfinder.batterymaterials.info/
14. *Jain H., Nowick A.S.* // Phys. Status Solidi. A. 1981. V. 67. P. 701. https://doi.org/10.1002/pssa.2210670242
15. *Hartmann E., Kovács L.* // Phys. Status Solidi. A. 1982. V. 74. P. 59. https://doi.org/10.1002/pssa.2210740105